Proceedings of the 20th International Conference on Soil Mechanics and Geotechnical Engineering– Rahman and Jaksa (Eds)

Two types of water absorption failure mechanism of unsaturated silt triaxial specimen

Deux types de mécanisme de rupture par absorption d'eau pour des échantillons triaxiaux de limon insaturé

Toshihiro Noda & Takahiro Yoshikawa
Department of Civil Engineering, Nagoya University, Japan, noda@nagoya-u.jp

ABSTRACT: Two types of triaxial experiments and their numerical simulations were performed. In the experiments, unsaturated silt specimens with suction 20 kPa were made to absorb water by (A) reducing suction to 0 kPa at a constant axial load higher than the peak value and by (B) reducing suction to 0 kPa, followed by raising pore pressure at another constant axial load lower than the peak value. Both specimens reached failure with water absorption showing the rapid increase of their axial displacement. A soil-water-air coupled finite deformation analysis code taking into account inertia force was employed for their numerical simulations. In the simulations, axial displacement did not converge during the water absorption and the specimen showed failure at an accelerated rate as seen in the experiments. In addition, it was found that the specimen behavior for case (A) showed softening with plastic volume compression due to increase in saturation degree, and the specimen behavior for case (B) showed softening with plastic volume expansion above the critical state line in $p' - q$ skeleton stress space.

RÉSUMÉ : Nous avons effectué deux types d'essais expérimentaux triaxiaux et leurs simulations numériques. Dans ces expériences, des échantillons de limon insaturé avec une aspiration de 20 kPa ont été amenés à absorber de l'eau en (A) réduisant l'absorption à 0 kPa avec une charge axiale constante supérieure à la valeur de crête, et en (B) réduisant l'absorption à 0 kPa, puis en augmentant la pression interstitielle à une autre charge axiale constante inférieure à la valeur de crête. Nous avons utilisé un code d'analyse des déformations finies couplées sol-eau-air qui prend en compte la force d'inertie pour les simulations numériques. Dans les simulations, le déplacement axial n'a pas convergé pendant l'absorption d'eau, et l'échantillon a montré une rupture à une vitesse accélérée, comme on le voit dans les essais. En outre, nous avons constaté que le comportement des échantillons pour le cas (A) montrait un ramollissement avec une compression de volume plastique en raison de l'augmentation du degré de saturation, et le comportement des échantillons pour le cas (B) montrait un ramollissement avec une expansion du volume plastique au-dessus de la ligne d'état critique dans l'espace de contraintes du squelette $p' - q$.

KEYWORDS: water absorption failure, soil-water-air coupled dynamic finite deformation analysis, unsaturated triaxial test.

1 INTRODUCTION

In recent years, there have been many collapses of slopes and embankments due to the heavy rain. Causes of collapse are considered as saturation of unsaturated soil, reduction of strength due to rise in pore pressure, and increase of self-weight due to water absorption, but the collapse mechanisms have not been completely elucidated. Normally, a combination of seepage flow analysis and stability analysis is used to predict the collapse of slopes and embankments in heavy rainfall. However, to comprehend the collapse mechanisms of ground and earth structures, it is insufficient to perform a stability analysis that determines whether the safety factor exceeds 1 or not, using the stress state obtained from a seepage flow analysis. It is necessary to have a mechanical system which can analyze ground and earth structures from deformation to failure caused by seepage. In addition, the failure phenomena are accompanied by acceleration motions even if the external force is rainfall. Therefore, it is necessary to take into consideration inertial forces. Furthermore, in order to simulate the large deformation behavior that leads to collapse, it is essential to consider the geometric nonlinearity based on finite deformation theory.

With the above background in mind, two types of experiment were performed where unsaturated silt triaxial specimens deformed to fail due to water absorption, together with their numerical simulations using the soil-water-air coupled finite deformation analysis code taking into account inertia force (Noda & Yoshikawa 2015). From the results, it was concluded that the two types of softening behavior greatly contribute to water absorption failure of unsaturated soil specimens.

2 EXPERIMENTAL AND ANALYTICAL CONDITIONS

2.1 *Experimental conditions*

In the triaxial test apparatus used in the experiments, the water pressure was controlled using a microporous membrane (Nishimura et al. 2012) on the bottom end of the test specimen, and the air pressure was controlled using a water repellant Polyflon filter on the top end. A double-cell system was used, and the volumetric changes were calculated from the change in water level of the inner cell.

The soil specimens used in the experiments comprised non-plastic silt (DL clay, soil particle density 2.70). The unsaturated triaxial specimens were subjected to two types of water absorption failure test, indicated as A and B below.

Test A Test of Water Absorption Failure Caused by Reducing Suction

This experiment supposed the saturation process in unsaturated ground or earth structures by rainfall and was performed by the following procedure: (i) Soil samples with water content adjusted to 25% were compacted statically in a mold to yield a cylindrical specimen (diameter of 50 mm and height of 100 mm) with the void ratio of 1.04 and the degree of saturation of 65%. (ii) The specimens were placed in the triaxial test apparatus under exhausted and undrained conditions, and the cell pressure was increased to 800 kPa (net stress 800 kPa). (iii) The air pressure was increased to 600 kPa (net stress 200 kPa). At this time, the water pressure measured at the bottom end of the specimen was 580 kPa (suction 20 kPa), and the void ratio was 0.85. Then the water pressure was adjusted and the drained condition was changed without changing suction of the specimen. (iv) Triaxial compression process was conducted at a constant

rate of axial load of 0.8 N/min under constant cell pressure and exhausted and drained conditions until the axial strain was 15%. (v) The water pressure was increased to 600 kPa (suction 0 kPa) while maintaining a constant axial load, and water absorption failure was induced. Note that separate from this experiment, the water pressure was adjusted after procedure (iii), and exhausted and drained triaxial compression tests were performed with constant suction at 0 kPa and 20 kPa and an axial strain rate of 0.01%/min. The results of these experiments are described in Section 3.

Test B　Test of Water Absorption Failure Caused by Increasing Pore Pressure

This experiment supposed an increase in pore pressure due to further water absorption after saturation of unsaturated ground or earth structures due to rainfall, thus there is a reduction not only in suction but also in net stress. The procedure was as follows: Procedures (i) to (iii) were the same as for Test A. (iv) Triaxial compression process was conducted at a constant axial load rate of 0.8 N/min under constant cell pressure and exhausted and drained conditions until the axial strain was 4%. (v) The water pressure was increased to 600 kPa (suction 0 kPa) and water absorption was induced while maintaining a constant axial load. This stage did not lead to failure. (vi) The air pressure and water pressure were increased simultaneously (maintaining suction at 0 kPa) while maintaining a constant axial load, and water absorption failure was induced. The results of this experiment are described in Section 4.

2.2 *Analytical conditions*

The constitutive model for the soil skeleton incorporated in the soil-water-air coupled finite deformation analysis code taking into account inertia force (Noda & Yoshikawa 2015) is an elasto-plastic constitutive model taking into consideration the unsaturated effect (Yoshikawa & Noda 2020) in the SYS Cam-clay model (Asaoka et al. 2002) developed by the research group of the authors. In accordance with Kyokawa et al. (2009) and Zhang & Ikariya (2011), a method was introduced in which the intercept of the normal consolidation line (NCL) and the critical state line (CSL) in the v−lnp' relationship is higher when the degree of saturation is lower. First, an overview of the model is described.

The intercepts of the NCL and CSL at the maximum degree of saturation ($s^{\mathrm{w}}_{\max}$) of the soil water characteristic curve is defined as N and Γ, respectively, and the intercept at the minimum degree of saturation ($s^{\mathrm{w}}_{\min}$) is defined as $\mathrm{N_r}$ and Γ_{r}, respectively. Then the following equations are obtained by applying linear interpolation between the two intercept points as the functions of the degree of saturation (s^{w}).

$$\mathrm{N}(s^{\mathrm{w}}) = \mathrm{N} + \frac{s^{\mathrm{w}}_{\max} - s^{\mathrm{w}}}{s^{\mathrm{w}}_{\max} - s^{\mathrm{w}}_{\min}}\left(\mathrm{N_r} - \mathrm{N}\right) \tag{1}$$

$$\Gamma(s^{\mathrm{w}}) = \Gamma + \frac{s^{\mathrm{w}}_{\max} - s^{\mathrm{w}}}{s^{\mathrm{w}}_{\max} - s^{\mathrm{w}}_{\min}}\left(\Gamma_{\mathrm{r}} - \Gamma\right) \tag{2}$$

In this case, it is assumed that $\mathrm{N}(s^{\mathrm{w}})$−$\Gamma(s^{\mathrm{w}})$ is constant, in accordance with Zhang & Ikariya (2011). Then, application of the elasto-plastic laws according to Asaoka et al. (2002) results in the following equations.

$$\overset{\circ}{\boldsymbol{T}}{}' = \boldsymbol{E}\boldsymbol{D} - \Lambda \boldsymbol{E}\frac{\partial f}{\partial \boldsymbol{T}'} \tag{3}$$

Here,

$$\Lambda = \frac{\dfrac{\partial f}{\partial \boldsymbol{T}'}\cdot \boldsymbol{E}\boldsymbol{D} + \mathrm{Q}\dot{s}^{\mathrm{w}}}{\dfrac{\partial f}{\partial \boldsymbol{T}'}\cdot \boldsymbol{E}\dfrac{\partial f}{\partial \boldsymbol{T}'} + J\dfrac{\mathrm{MD}}{p'(\mathrm{M}^2 + \eta^{*2})}(\mathrm{M}_s{}^2 - \eta^2)} \tag{4}$$

$$\mathrm{Q} = \frac{\mathrm{N_r} - \mathrm{N}}{\mathrm{v}_0\left(s^{\mathrm{w}}_{\max} - s^{\mathrm{w}}_{\min}\right)}\ (>0) \tag{5}$$

where $\boldsymbol{E}$ is the elastic modulus tensor, $\boldsymbol{D}$ is the stretching tensor of the soil skeleton, Λ is the plastic multiplier, f is the plastic potential, $\boldsymbol{T}'$ is the skeleton stress tensor (Jommi 2000), and $\overset{\circ}{\boldsymbol{T}}{}'$ is the objective skeleton stress rate tensor. Note that the skeleton stress tensor $\boldsymbol{T}'$ is given by

$$\begin{aligned} -\boldsymbol{T}' &= -\boldsymbol{T} - (s^{\mathrm{w}}p^{\mathrm{w}} + s^{\mathrm{a}}p^{\mathrm{a}})\boldsymbol{I} \\ &= -\boldsymbol{T} - p^{\mathrm{a}}\boldsymbol{I} + s^{\mathrm{w}}(p^{\mathrm{a}} - p^{\mathrm{w}})\boldsymbol{I} \end{aligned} \tag{6}$$

where $\boldsymbol{T}$ is the total stress tensor, $\boldsymbol{I}$ is the identity tensor, p^{w} is the pore water pressure, p^{a} is the pore air pressure, $\boldsymbol{T}'$ and $\boldsymbol{T}$ are positive in tension, and p^{w} and p^{a} are positive in compression. $-\boldsymbol{T}-p^{\mathrm{a}}\boldsymbol{I}$ is the net stress tensor. Regarding the variables in Λ, J is det$\boldsymbol{F}$ ($\boldsymbol{F}$ is the deformation gradient tensor of the soil skeleton), M is the critical state constant, D is the dilatancy coefficient, p' is the mean skeleton stress, η is the stress ratio, and M_s is the threshold stress ratio between hardening and softening in the SYS Cam-clay model (Asaoka et al. 2002). Furthermore, Q is a new term added as a result of introducing the methods of Kyokawa et al. (2009) and Zhang & Ikariya (2011), and v_0 in Q represents the specific volume at the start of analysis. $\dot{s}^{\mathrm{w}}$ represents the material time derivative of the degree of saturation viewed from the soil skeleton, and its positive and negative contributes to hardening or softening behavior and the loading criterion, the same as for the stress rate. Specifically, from Prager's consistency condition, the following equations can be obtained:

$$\frac{\partial f}{\partial \boldsymbol{T}'}\cdot\dot{\boldsymbol{T}}' + \frac{\partial f}{\partial \boldsymbol{\beta}}\cdot\dot{\boldsymbol{\beta}} + \mathrm{MD}\frac{\dot{R}^*}{R^*} - \mathrm{MD}\frac{\dot{R}}{R} + \mathrm{Q}\dot{s}^{\mathrm{w}} = \dot{\varepsilon}^{\mathrm{p}}_{\mathrm{v}} \tag{7}$$

$$\frac{\partial f}{\partial \boldsymbol{T}'}\cdot\overset{\circ}{\boldsymbol{T}}{}' = \Lambda J\frac{\mathrm{MD}}{p'(\mathrm{M}^2 + \eta^{*2})}(\mathrm{M}_{\mathrm{s}}{}^2 - \eta^2) - \mathrm{Q}\dot{s}^{\mathrm{w}} \tag{8}$$

Therefore focusing on Q>0, it can be seen that when the soil is under loading conditions, the increase in the degree of saturation ($\dot{s}^{\mathrm{w}} > 0$) promotes plastic volume compression and softening. Note that $\dot{\varepsilon}^{\mathrm{p}}_{\mathrm{v}}$ in Eq. 7 is the plastic volume rate (positive in compression), $\boldsymbol{\beta}$ is the rotational hardening variable, R^* is the degree of structure, R is the degree of overconsolidation, and overdots indicate material time derivatives viewed from the soil skeleton. For details, refer to Asaoka et al. (2002).

The material constants for the constitutive model for the soil skeleton and the soil water characteristic model (Gallipoli et al. 2003) were determined by reference to the values for DL clay of Yoshikawa et al. (2015). Note that procedure (iii) in Section 2.1, which is shared in common in Tests A and B, was taken to be the initial condition, and simulation was performed using a set of material constants and initial values.

Figure 1 shows the finite element mesh and boundary conditions. For simplicity, the axial symmetry of the cylindrical specimen was assumed and the effect of gravity was ignored. To reproduce rigid and frictional cap conditions on the top end, constant length and constant angle constraint conditions (Asaoka et al. 1998; Noda et al. 2008) were applied between the nodes.

On the bottom end, as shown in Figure 1, pedestal conditions

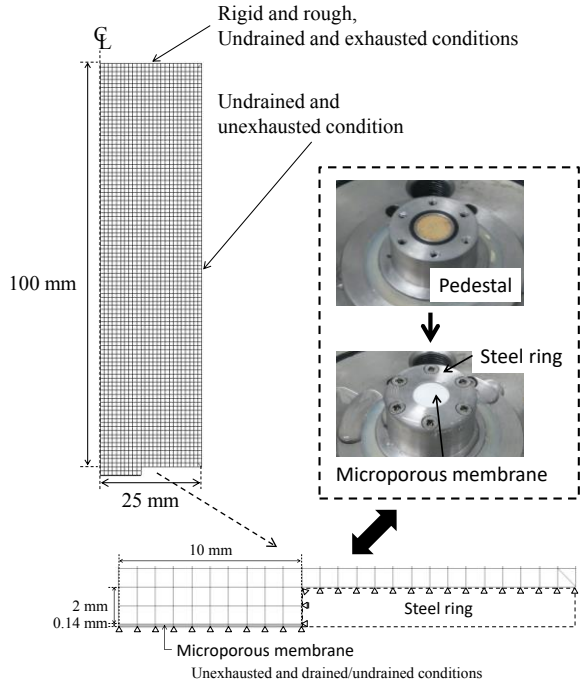

Figure 1. Finite-element mesh and boundary conditions.

with a microporous membrane fixed with a 2 mm thick steel ring were reproduced in detail. The microporous membrane was assumed to be a two-phase material that did not deform and was given the same coefficient of water permeability as the experimental value (7.0×10^{-8} m/s). The air and water boundary conditions were controlled at the top and bottom ends respectively in the same manner as in the experiments. During shearing, the bottom end was fixed in the vertical direction and compression was applied at the top end with the same axial load rate or axial displacement rate as in the experiments. The analytical results were displayed using the apparent elemental behavior in the same manner as in the experiment. That is to say, the axial load was calculated from the equivalent nodal reaction force of nodes at the upper edge of the specimen, and the skeleton stress was calculated counting the lateral pressure. The cross section was corrected assuming the specimen to be cylindrical. Axial strain was obtained by dividing the axial displacement by the specimen height immediately before shearing. The degree of saturation and volumetric strain was calculated by taking a volumetric average over the specimen by using the value of each element.

3 TEST OF WATER ABSORPTION FAILURE CAUSED BY REDUCING SUCTION (TEST A)

Figures 2 and 3 show the experimental and analytical results, respectively. First, from the displacement control experimental results with an axial strain rate of 0.01%/min and constant suction (0 kPa and 20 kPa), it was found that the strength and stiffness were higher for 20 kPa suction than for 0 kPa, and the analytical results were also able to reproduce this difference. This is because according to the elasto-plastic constitutive model as described in Section 2.2, the degree of saturation was lower with 20 kPa suction, so the strength and stiffness were greater.

Next, the test in which the suction was reduced from 20 kPa to 0 kPa while maintaining the axial load constant after triaxial compression up to an axial strain of 15% is described. First, in the experiment, the degree of saturation increased with water absorption due to the reduction of suction, and an increase in axial displacement and reduction in deviator stress (softening) were observed. At this time, although the axial load was maintained constant, the corrected cross-sectional area increased with increase in axial displacement and decrease in volume, so the deviator stress was reduced. Finally, the experiment was terminated when the axial strain reached 25%, corresponding to the stroke limit of the test apparatus, without convergence of the axial displacement. On the other hand, in the analysis, the degree of saturation increased with water absorption due to the reduction in suction; the axial displacement increased and deviator stress decreased (softening); and the axial strain exceeded 25% without convergence.

Figure 4 shows a comparison of the experiment and analysis for the variation of the axial strain with time after reducing suction from 20 kPa to 0 kPa. In the experiment, axial displacement occurred rapidly within about one minute after reducing suction, and this was also reproduced well in the analysis. Figure 5 shows the variation with time of the velocity and acceleration of the top end of the specimen in the analysis.

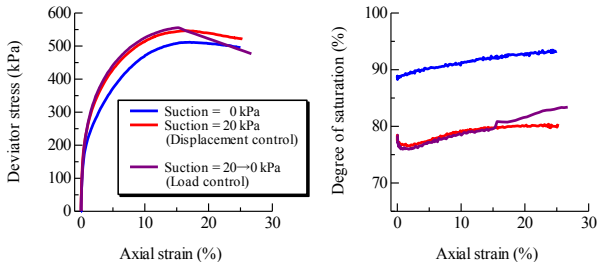

Figure 2. Experimental results for water absorption failure caused by reducing suction.

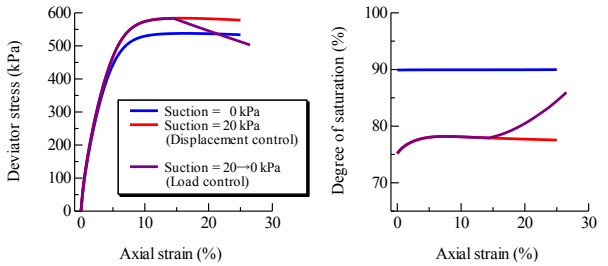

Figure 3. Analytical results for water absorption failure caused by reducing suction.

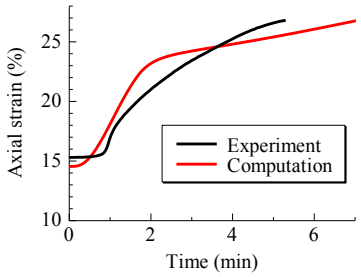

Figure 4. Increase of axial displacement after reducing suction.

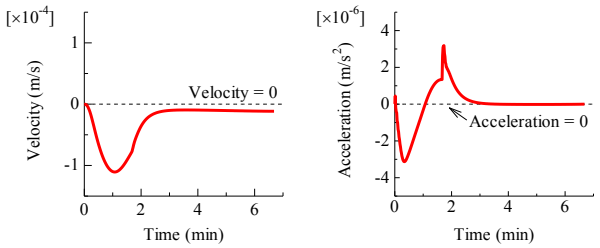

Figure 5. Analytical results for velocity and acceleration after reducing suction (leading to failure accompanied with acceleration).

The velocity increased immediately after reducing suction, and the specimen exhibited motion with acceleration. Therefore,

the water absorption failure behavior observed in the experiment was reproduced, thus a deformation analysis code taking into consideration inertial forces is essential.

4 TEST OF WATER ABSORPTION FAILURE CAUSED BY INCREASING PORE PRESSURE (TEST B)

In the previous section, the water absorption failure test in which the axial load was maintained constant at an axial strain of 15% and suction was reduced was described. In this section, the water absorption failure test in which the axial load was maintained constant at the comparatively small axial strain of 4% (at the stage before the deviator stress peak of the exhausted and drained test in Figure 2) is described. Figures 6 and 7 show the experimental and analytical results, respectively. Figure 8 shows a comparison of the experiment and analysis for the variation of the axial strain with time after reducing suction from 20 kPa to 0 kPa at an axial strain of 4%. As shown in Figure 8, after reducing the suction to 0 kPa, the net stress was reduced from 200 kPa to 190 kPa and then to 180 kPa, continuing to be reduced further thereafter, as a result of simultaneously increasing the air

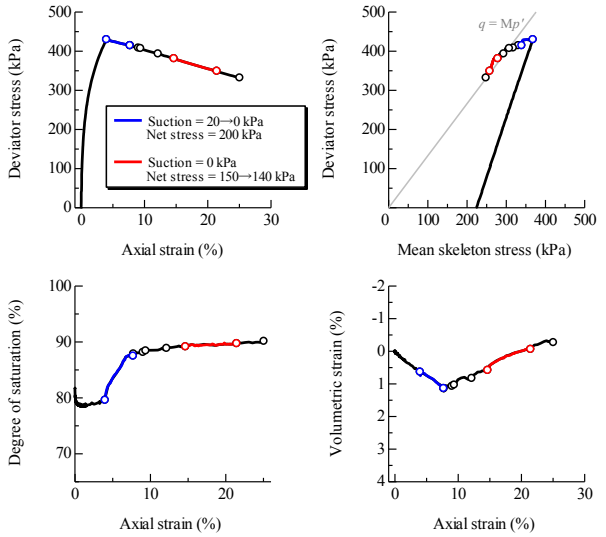

Figure 6. Experimental results for water absorption failure caused by increasing pore pressure.

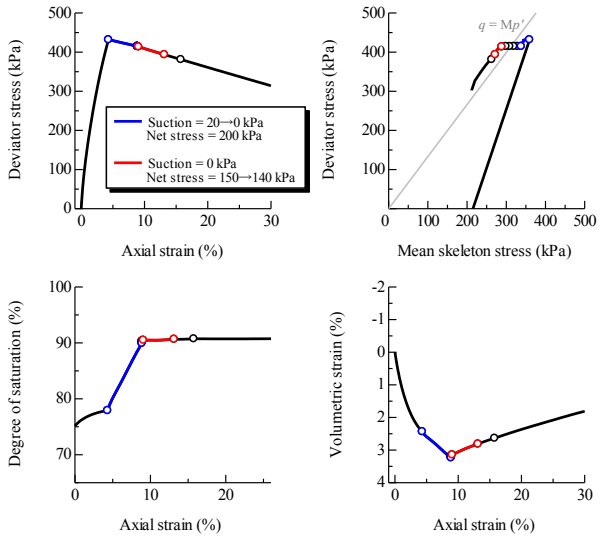

Figure 7. Analytical results for water absorption failure caused by increasing pore pressure.

pressure and water pressure (maintaining the suction at 0 kPa). Note that the experiment was terminated when the test apparatus reached its stroke limit at an axial strain of 25%, which was at about a net stress of 135 kPa, but analysis was performed down to a net stress of 115 kPa. In each figure, ○ indicates the starting point for each stage (the end point of the previous stage).

First, by comparing the experimental result in Figure 6 and the analytical result in Figure 7, it can be seen that the analytical result reproduces well the characteristics of the experimental result. In particular, in the stage in which suction is reduced from 20 kPa to 0 kPa (indicated in blue in the figures) and the stage in which the net stress is reduced from 150 kPa to 140 kPa as the pore pressure is increased (indicated in red), there is a large increase in axial displacement in both the experiment and analysis, and significant softening behavior is exhibited. Also, volume compresses with the increase in the degree of saturation during the stage of suction reduction, but the degree of saturation does not change during the stage of the pore pressure increase, and the volume expands. This is because, as stated in Section 2.2, the stage of suction reduction exhibits softening behavior with plastic volume compression due to the increase in the degree of saturation, whereas in the stage in which pore water pressure is increased and net stress is reduced from 150 kPa to 140 kPa, softening behavior with plastic volume expansion is exhibited in the effective stress (skeleton stress) state on the upper side of the critical state line ($q = Mp'$), which is a characteristic of the Cam-clay model. Figure 9 shows the loading conditions within the specimen in the stage in which suction is reduced and in the stage in which the net stress is reduced from 150 kPa to 140 kPa. As stated above, the former is softening behavior with plastic volume compression, and the latter is softening behavior with plastic volume expansion; this demonstrates that there are two different water absorption softening mechanisms in the specimen.

In addition, from Figure 8, it can be seen that axial displacement occurs rapidly in the final stage and that this motion is accompanied with acceleration, as described in Section 3.

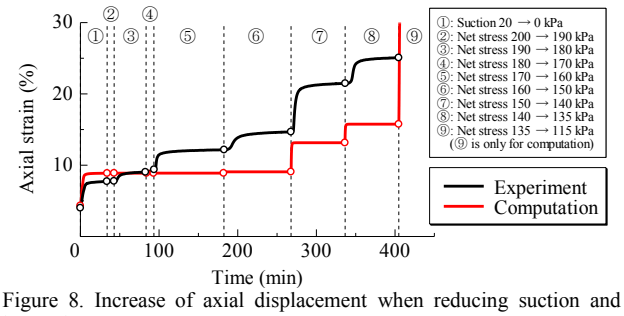

Figure 8. Increase of axial displacement when reducing suction and increasing pore pressure.

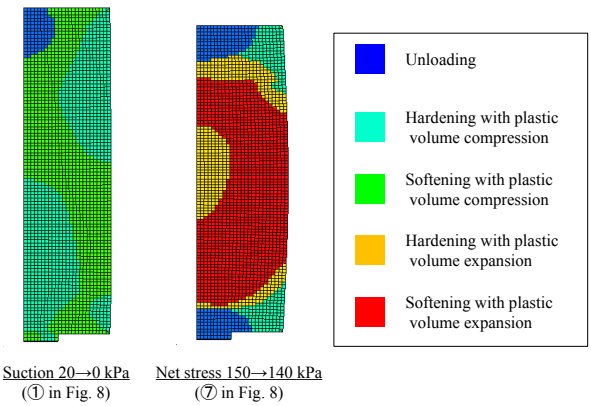

Figure 9. Comparison of loading conditions within the specimen.

5 CONCLUSIONS

In this paper, two types of water absorption failure test were

performed on unsaturated silt triaxial specimens under the constant axial load condition, as described below, focusing on the peak deviator stress obtained in a displacement-controlled triaxial compression test with suction of 0 kPa, and the experiment results were compared with numerical simulation results. In Test A, suction was reduced (degree of saturation increased) while maintaining a constant load in the stage after the peak, and in Test B, suction was reduced to 0 kPa while maintaining a constant load in the stage before the peak, and then the pore pressure was raised. In both Test A and B, the specimen exhibited water absorption softening, and axial displacement rapidly increased, leading to failure. In the numerical simulations, we succeeded in reproducing the behavior leading to failure with acceleration when the specimens absorbed water, using a soil-water-air coupled finite deformation analysis code taking into account inertial force (Noda & Yoshikawa 2015). From the comparisons, it was found that Test A showed softening behavior with plastic volume compression caused by an increase in the degree of saturation (decrease in suction), as described in the constitutive model that takes the unsaturated effect into consideration, whereas Test B showed softening behavior with plastic volume expansion above the critical state line in p'–q ($=\eta p'$) space (a characteristic of the Cam-clay model).

In the future, we would like to examine the water absorption failure mechanisms in real ground or earth structures.

6 ACKNOWLEDGEMENTS

This work was supported by JSPS KAKENHI Grant Number JP17H01289.

7 REFERENCES

Asaoka, A., Noda, T. and Kaneda, K. 1998. Displacement/traction boundary conditions represented by constraint conditions on velocity field of soil, *Soils and Foundations*, 38(4), 173-181.

Asaoka, A., Noda, T., Yamada, E., Kaneda, K. and Nakano, M. 2002. An elasto-plastic description of two distinct volume change mechanisms of soils, *Soils and Foundations*, 42(5), 47-57.

Gallipoli, D., Wheeler, S.J. and Karstunen, M. 2003. Modelling the variation of degree of saturation in a deformable unsaturated soil, *Géotechnique*, 53(1), 105-112.

Jommi, C. 2000. Remarks on the constitutive modelling of unsaturated soils, *Experimental Evidence and Theoretical Approaches in Unsaturated Soils* (Tarantino, A. and Mancuso, C. eds.), Balkema, 139-153.

Kyokawa, H., Kikumoto, M., Nakai, T. and Shahin, H.M. 2009. An elasto-plastic constitutive model for unsaturated soil unified considering the relation between suction, degree of saturation and density, *Journal of Applied Mechanics*: JSCE, 12, 331-342. (in Japanese)

Nishimura, T., Koseki, J., Fredlund, D.G. and Rahardjo, H. 2012. Microporous membrane technology for measurement of soil-water characteristic curve, *Geotechnical Testing Journal*, the American Society for Testing and Materials, 35(1), 201-208.

Noda, T., Asaoka, A. and Nakano, M. 2008. Soil-water coupled finite deformation analysis based on a rate-type equation of motion incorporating the SYS Cam-clay model, *Soils and Foundations*, 48(6), 771-790.

Noda, T. and Yoshikawa, T. 2015. Soil-water-air coupled finite deformation analysis based on a rate-type equation of motion incorporating the SYS Cam-clay model, *Soils and Foundations*, 55(1), 45-62.

Yoshikawa, T., Noda, T. and Kodaka, T. 2015. Effects of air coupling on triaxial shearing behavior of unsaturated silty specimens under constant confining pressure and various drained and exhausted conditions, *Soils and Foundations*, 55(6), 1372-1387.

Yoshikawa, T. and Noda, T. 2020. Triaxial test on water absorption compression of unsaturated soil and its soil-water-air-coupled elastoplastic finite deformation analysis, *Soils and Foundations*, 60(5), 1151-1170.

Zhang, F. and Ikariya, T. 2011. A new model for unsaturated soil using skeleton stress and degree of saturation as state variables, *Soils and Foundations*, 51(1), 67-81.